AUTOMATIC DETECTION OF CHANGES AND DEFORMATIONS IN ROCK FACES BY TERRESTRIAL LASER SCANNING

M. Alba, M. Scaioni

Politecnico di Milano, Dept. of Building Environment Science & Technology, via M. d'Oggiono 18/a, 23900 Lecco, Italy - e-mail: {mario.alba, marco.scaioni}@polimi.it

Commission V, WG V/3

KEY WORDS: Terrestrial Laser Scanning, Deformation Monitoring, Change Detection, Rockfall, Digital Surface Analysis, Vegetation filtering

ABSTRACT:

The use of TLS application for forecasting of possible rock falls is the main aim of this research, whose intermediate steps have been already presented in previous publications. Through some experiences carried out in monitoring of a few rock faces in Italian Prealps, the whole process to extract changes and to detect deformations of their shape along time is outlined. All the steps of the processing pipeline are here described. First, problems concerning setting up of the reference system, data acquisition and reduction of georeferencing errors are analyzed. Second, the use of a low-cost NIR camera integrated to a terrestrial laser scanner for filtering out vegetation from point clouds is proposed and a test presented. Finally two algorithms able to automatically recognize changes (i.e. rock mass detached) and deformations between surfaces acquired at different epochs are presented and discussed.

1. INTRODUCTION

The problem of preventing or reducing damages due to rock falls is complex, because of to the very large number of feasible scenarios with the local morphology of the site providing an additional degree of freedom. Today the interest of researchers is focusing on the application of terrestrial laser scanning (TLS) for monitoring and understanding of on-going millimetric deformations that can be a signal of forthcoming failures (Abellán *et al.*, 2006). This task is really complex, due to the need of measuring displacements smaller than the uncertainty of TLS measurements. In recent years, different area-based techniques have been applied to exploit the data redundancy achievable by laser scanning measurements in order to improve the precision (see e.g. Lindenbergh and Pfeifer, 2005; Schneider, 2006; Abellán *et al.*, 2006). On the other hand, such methods require regular surfaces to be interpolated by analytical functions, at least at local level, and unfortunately this assumption rarely holds when dealing with rock cliffs. In addition, major changes of the rock shape might occur during two observation epochs, resulting in a significant modification of the surface where deformations are investigated. One kind of changes is represented by rocks that detached from the cliff. The evaluation of the amount and the spatial distribution of detachments is not only a prerequisite for the deformation analysis, but it's a task that yields an important additional information, very useful to evaluate the real magnitude of rock fall events in a given location. Unfortunately, loss of material and deformation of the rock face's surface might occur at the same time and can be of similar magnitude. A method for efficient deformation analysis should be able to take apart both processes. In addition, vegetation frequently grows on the cliff and roughly modify the surfaces detectable by TLS survey. Obviously, if the surface covered by bushes is too wide, this will prevent any monitoring activity. In fact, even if a TLS capable of recording multiple echoes of the laser returns is used (e.g. the Riegl VZ-400), a too much dense leaves layer cannot be partially penetrated. On the other hand, in case vegetation marginally covers the rock face, analyses will be able to be pursued only after filtering.

The paper describes a whole pipeline to extract changes and deformation detection between two (or more) digital surfaces of the same rock face surveyed at different observation epochs by using a TLS (see Fig. 1). Analysis is based on three main steps: (i) vegetation filtering based on NIR imagery; (ii) detection of major changes, i.e. loss of material; (iii) deformations analysis and testing.

In a previous paper (Alba *et al.*, 2009), the problem of *laser scan georeferencing* was afforded. Here a procedure to get multi-temporal point clouds georeferenced in the same reference system was presented, task which represents a fundamental prerequisite to the deformation analysis process. Outcomes and practical issues about data acquisition will be outlined in section 2.

A second preliminary aspect is related to *vegetation filtering*. In the abovementioned paper, a few spatial filters were tested, but results were not satisfactory at all. The complexity of the rock surface and the irregular growth of bushes was a relevant obstacle to their successful application. An alternative approach based on the use of a low-cost NIR camera to discriminate vegetation from the rock background will be dealt with in section 3. This task is a preliminary stage to prepare both rock surfaces to the comparison to detect deformations and changes (Sect. 4). Some results obtained from the application of the pipeline described in figure 1 to a test site located in Italian Prealps will be reported in section 5.

2. DATA ACQUISITION AND LASER SCAN GEOREFERENCING

For any monitoring operation the setup of a stable reference system is fundamental to compare scans taken at different epochs. Problems concerning the data acquisition and the reduction of georeferencing errors were already analysed and discussed in Alba *et al*. (2009).

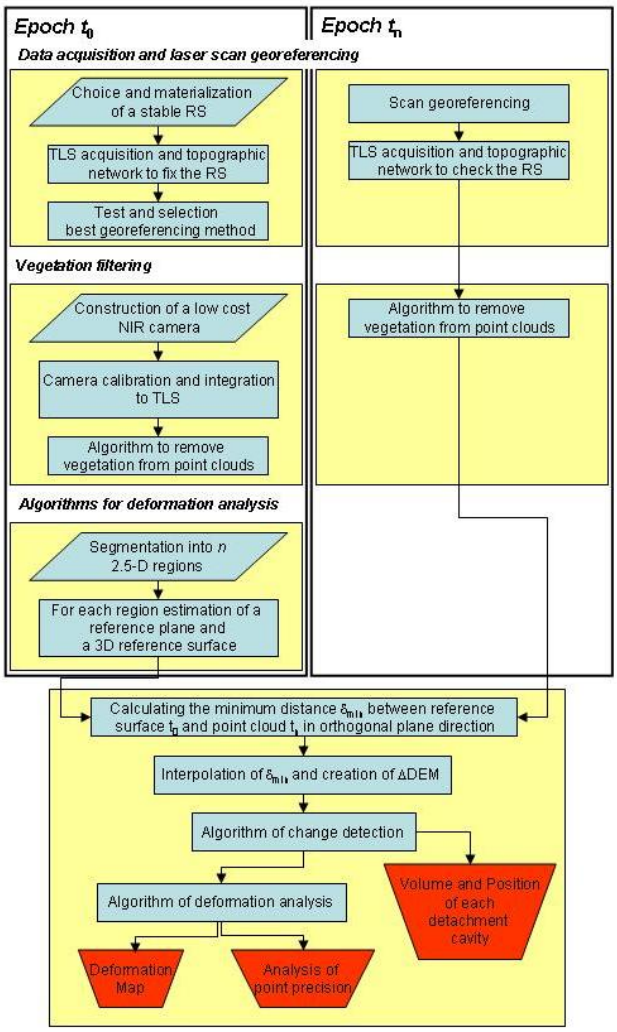

Fig. 1 Workflow of the rock fall monitoring pipeline

During the experimental tests, the *ground reference system* (GRS) was presented by a local geodetic network consisting on a few monuments. A removable steel pillar could be repositioned at each observation epoch on one or more points, in order to setup the laser scanner in the same position with high precision. The TLS accurate repositioning has the advantage that multi-temporal scans can be captured through the same geometric scheme, thus some systematic errors occur the same way (e.g. the ones related to the angle of incidence of the laser beam with respect to the rock face surface) and can be removed when two scans are subtracted each from the other. Furthermore, the 3D position of the centre of the *intrinsic reference system* (IRS) of the instrument could be constrained to the same 3D point. The remaining DoF were fixed according to a couple of different strategies. In case of short distance between the TLS stand-point and the rock face (tens of metres), some retro-reflective targets (RRT) placed on the cliff allowed to compute the rotation matrix of the IRS. The use of such targets introduce systematic errors due to their measurement, that can be partially corrected by using some empirical models (see e.g. Alba *et al.*, 2008). In case of longer distances, the application of a *surface matching* algorithm (ICP) was applied to compute the unknown rotations of the IRS.
The measurement of the vertices of the geodetic network is repeated at each epoch to assess their stability. The use of a redundant scheme and the short distances involved allowed to obtain high precisions in 3D point determination, less than ±1 mm for all TLS stand-points and targets.
The laser scanning survey was carried out in the test-field by using a ToF instrument Riegl LMS-Z420i. In all measurement sessions the same scanning parameters and acquisition windows were adopted. In order to improve the precision, each scan was acquired in 'multiscan' mode, i.e. it was repeated 4 times.
Also in this case, more information can be found in Alba *et al.* (2009), where these issues are discussed in detail.

3. VEGETATION FILTERING

A recurrent problem occurring in rock slopes analysis is due to the presence of vegetated areas which prevent the acquisition of the bare cliff surface. The problem of the vegetation reduction on rock faces is more complex than it usually is with airborne laserscanning (ALS) data. First, bushes on a cliff grow in a direction that is quite parallel to that of the face itself, not orthogonal likewise trees in ALS data. This makes really difficult its automatic recognition. On the other hand, also the kind of vegetation growing on the cliff might influence the result of the recognition process. For example, turf grass is hardly distinguishable from the background. In Alba *et al.* (2009) some techniques that can be applied for removing vegetation from point-clouds are presented and analysed. Unfortunately, the morphological complexity of a rock face results in the outcome that is very difficult to obtain satisfactory results with semi-automated filters. For this reasons a new automatic system based on a *high resolution near infrared* (NIR) camera able to identify vegetation was designed. The near infrared is an electromagnetic radiation with a wavelength lower than visible light, but greater than that of thermal radiation, which are in the range 750-1400 nm. NIR images are usually used in the common practice of satellite-borne remote sensing since many years (Turker, 1979). The proposed methodology is the transposition of these state-of-the-art techniques to the analysis of rock faces. The ultimate goal is to discriminate and eliminate from all points clouds to compare all the areas covered by vegetation. The process to carry out this is expected to be fast and highly automated, without requiring subsequent filtering operations.
Several expensive commercial NIR sensors are sold today, but the solution adopted here has been to construct a low-cost camera (Subsect. 3.1) by modifying a consumer SLR camera.
In the following subsections the integration and calibration of the NIR camera to TLS (Subsect. 3.2), and the filtering algorithm to recognise and remove vegetated areas (Subsect. 3.3) are presented.

3.1 Construction of a low-cost NIR camera

In the market there is a wide range of sensors to enable acquisition of NIR image according to sensor resolution and wavelength. The choice of the camera to be used was influenced by several factors:

- the sensor resolution accompanied by the use of interchangeable lenses should ensure the acquisition of images with a resolution close to that of the TLS;
- to ensure a automatic integration of its data with TLS system;
- to reduce the hardware cost.

For these grounds the choice fell on using a modified SLR digital camera, which was amended to allow the NIR band acquisition.

Digital cameras are generally equipped with a matrix of CCD (or CMOS) sensors that have a very broad spectral response, throughout the visible and near infrared. Manufacturers introduce two different filters in front of the sensor to prevent the acquisition of the NIR band and to improve the colour quality. The former filter is actually made up a series of microfilters of alternate colors (RGB), each of which is positioned in front of each CCD sensor according to a specific scheme (e.g. that of Bayer). Thus the signal that hits a single CCD contains only the component corresponding to the microfilter colour. The latter filter is used to reduce the effect of the infrared component of the signal and it is placed in front of the whole sensor. This filter, unlike RGB color microfilters, can be replaced.
A digital camera Nikon D100 was used to test the procedure. The filter placed in front of the infrared sensor was replaced with another one (black) that stops all visible wavelengths and allows to go through the NIR component only. In figure 2 the characteristics of the original filter bandwidth compared with the theoretical effect of black filter is showed. Replacement operations (see Fig. 3) were performed as indicated by *lifepixel* (www.lifepixel.com).

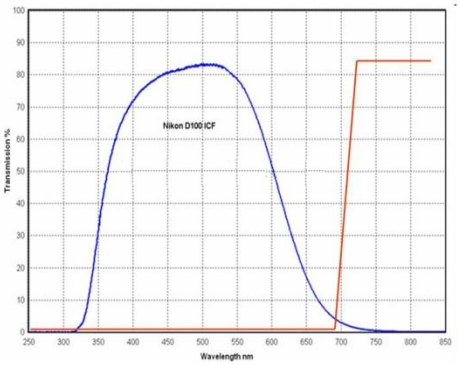

Fig. 2. In blue color the original filter characteristics, in red the theoretical effect of black filter.


Fig. 3. Replacement operation of black filter

3.2 Camera calibration and integration to TLS

Once the replacement of the black filter in the Nikon D100 camera had been ended and checked out, a standard camera calibration was performed. The intrinsic calibration of the camera, needed to determine the parameters of inner orientation and distortion coefficients (according to the model of Brown, but limited to 8 coefficients), was performed using the calibration tool of the commercial software PhotoModeler ver. 6 by EOS Systems, Canada (www.photomodeler.com). It should be noted the use of calibration frames based on coloured targets is prevented, because the NIR sensor will be unable to take apart symbols from the background.
The computed distortion parameters were directly implemented in the acquisition software of laser scanner (Riscan Pro, Riegl). The low-cost NIR camera was mounted above the laser head and oriented with respect to the IRS by using a standard procedure normally adopted with digital camera in the visible range. This procedure involves the use of some RRT and the acquisition of one image and one laser scan. Past investigations have found some misalignment between images and scan if the calibration was performed using a single image, probably due to an imperfect alignment with the rotation axis of the instrument. For this reason, the calibration was performed using a polygon with RRT places around the instrument within a 360° field. Obviously the estimated residuals on the image are greater but allow better alignment of images for all angles of acquisition.
From now on each NIR image can be automatically oriented in the IRS and then mapped onto point clouds.

3.3 Algorithm to remove vegetation from point clouds

After the calibration of the sensor first images were acquired to verify the proper application and to analyze the first datasets. The field lab called ‘cliff B’ in the test site described in Alba *et al.* (2009) was used. Here a new scan and new NIR images were captured with either the modified NIR camera mounted on the TLS, and some other by hand-held camera. Indeed, the second set of images was focused to acquire some details of vegetation grown on the rock face. The test was carried out in december 2009, when the development of vegetation on the rockface was very limited.
The strategy of the algorithm for vegetation filtering is: (i) to discriminate the vegetation from the rest of cliff surface, task that is carried out on the NIR images; for each of them a binary mask is created, which permits to classify its content as vegetation or background; (ii) classified images are projected onto the 3D scan, so that each 3D point can be classified as vegetation or rock background; the former points are filtered out, the latter are used for next processing stages.
Images captured by the camera used, although recorded on the three classical channels RGB are really monochromatic on the single NIR band. In each RGB channel slightly different wavelength is recorded because of the colour filter placed in front of the sensor, as showed in figure 4. These differences could be exploited by using some kind of vegetation index, but these would require a preliminary characterization of each RGB channel to make their use more effective (Labbè *et al.*, 2007). For this reason, at the moment we preferred a method that uses one channel only. First for each image a stretching algorithms that saturates each RGB channel was applied, thereby increasing contrast (Fig. 4). Then the images corresponding to each band were converted to greyscale and a threshold on the intensity value was applied to classify pixels as vegetation or rock. As can be seen in figure 5, a set of binary masks originated from different RGB band images are worked out. Finally, to improve the binary classification process, two filters are applied. The first one fills any holes that was not been measured inside an area recognized as vegetation. The second eliminates all single pixels in the binary images by applying a median filter. Indeed, single pixels which stand out from the background are considered as outlier. The resulting mask replaced the original one, so that all points corresponding to vegetation in the point cloud can be removed.
As anticipated, a first data acquisition was perfomed in the month of december 2009, when the vegetation growth was very early. For this reason, testing of the algorithms on the entire

rockface could not be completed, but will be during next summer.

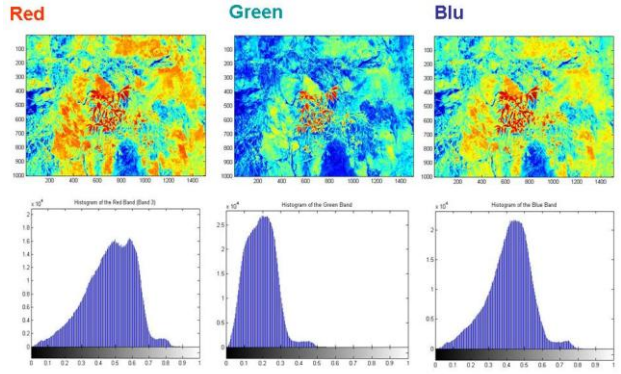

Fig. 4. The images shows the contents of each RGB bands and the relative histograms.

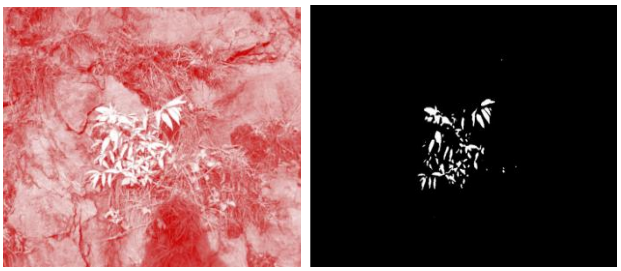

Fig. 5. On the left the NIR image, on the right the final mask with classified pixels as vegetation (white) or rock background (black).

4. ALGORITHMS FOR DEFORMATION ANALYSIS

The basic concept that was followed here is to exploit the data redundancy of a point-cloud to improve the precision of detectable deformations. In fact, the aim in this phase is to recognize areas where the shape of the rock surface has changed significantly, or where rocks have fallen down. In particular the interest is focused on detection of small size deformations and rock falls, in the order of a few millimetres for the former, and a few centimetres for the latter ones, respectively. Because the magnitude of the quantities to be detected is very close or also lower to the uncertainty of TLS measurements, a simple comparison between both point clouds, as done in the case of ground slope landslides (see e.g. Teza *et al.*, 2007) is not enough.

However, the application of the area-based analysis to rock faces is more complex than it is in case of man-made structures, due to the presence of irregular surfaces which prevent from the interpolation with analytical functions. In addition, here the chance of major changes also has to be considered.

To cope with this problem the method proposed by Lindenbergh and Pfeifer (2005) has been extended to the case of irregular surfaces, like rock faces usually are. More details on the algorithms, that is outlined in figure 1, can be found in Scaioni and Alba (2010).

4.1 Preliminary data processing

The area of a rock face to be analysed might be very wide and feature a complex shape. The algorithms described in the following work on surfaces which can be interpolated with respect to a reference plane (2.5-D region). Each of them is referred to as 'Interested Region *k*-th' ($IReg_k$) and will be analyzed separately afterwards. If this requisite is not directly satisfied, the whole point cloud will need to be segmented into several 2.5-D regions. Here only the point cloud captured at the first epoch is segmented, and then the same subdivision will be applied the same on the following datasets. The segmentation is carried out by using a RANSAC technique as proposed by Roncella and Forlani (2005). Results obtained for the 'cliff B' addressed in subsection 3.3 is reported in figure 6. In case a cliff was surveyed by using more laser scans, the segmentation and the next deformation analysis can be performed on each of them separately from the others. This solution eliminates errors to scan mutual registration.

Finally, portion of the captured point cloud(s) is resampled to a square grid lattice (DEM), whose step δ_{DEM} is very close to the original data resolution to avoid loss of information content. The data resampling to give out a regular DEM however introduces errors due to data modelling, which are larger in case of corrugated surfaces. For this reason, the selection of a suitable step fo DEM δ_{DEM} is crucial. On the other hand, this step cannot be avoided, because comparison between two point cloud cannot be performed pointwise.

Finally, preprocessing is ended by subtracting both DEMs corresponding to a pair of observation epochs to be compared. The resulting DEM of differences (ΔDEM) in each $IREG_k$ is expected to be a more regular and flat region, especially in absence of changes and deformations.

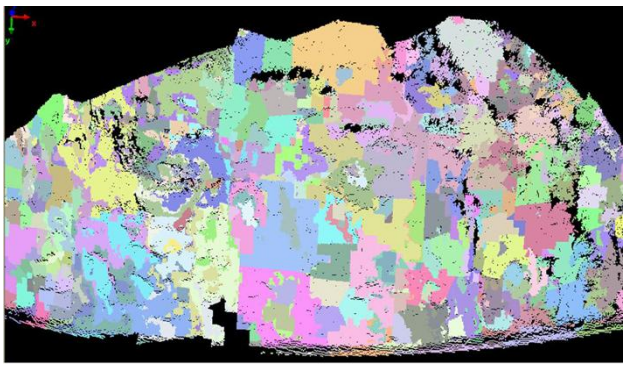

Fig. 6. Results of the segmentation into 2.5-D regions of the point cloud surveyed at test site 'cliff B.'

4.2 Algorithm of change detection

Changes on a rock face are for the most due to detachments of boulders or to the vegetation mass variation. Both feature either specific characteristics that allow to recognize them, and some others that are undifferentiated. For example, rockfalls result in a negative change on the ΔDEM, while vegetation gives rise to positive changes during its growth and negative when leaves fall. On the other hand, vegetation is supposed to be filtered out by processing NIR images (Sect. 3).

The procedure that is described tries to extract information from the ΔDEM according to a set of basic rules. First of all, rock detachments are the unique negative changes (holes) on the ΔDEM. Secondly, only masses of significant size are considered, because the ones featuring a smaller size are not relevant for the geological analysis. To recognize holes in the ΔDEM two thresholds have been introduced: the *minimum width* (w_{cav}) of a rock-mass which has detached and the *minimum depth* (δz_{cav}) of the resulting cavity. Obviously the minimum cavity depth must be larger than the minimum deformation that can be detected ($\delta z_{cav} > \delta z_{def}$).

The basic concept of the change detection algorithm is to perform an analysis of volumetric changes by considering relevant variations in the ΔDEM surface. The assumption made

is that changes are much larger that data uncertainty and they can be detected by fixing suitable thresholds depending on the geomorphology of the cliff. The localization of holes is carried out in the following two phases.

4.2.1 Holes localization. The convolution of the matrix describing the ΔDEM with an averaging mask **H** (side *w*) is computed to find the map (**M**) of local peaks:

$$\mathbf{M} = \mathbf{\Delta DEM} \otimes H = \mathbf{\Delta DEM} \otimes \frac{1}{w^2}\mathbf{I}_{wxw} \quad (1)$$

Secondly, each element of **M** is tested to check if it belongs to a region of detachment:

$$\forall i,j \in \mathbf{M} \begin{cases} D_{i,j} = 1 & when\ M_{i,j} < \delta_{zcav} \\ D_{i,j} = 0 & elsewhere \end{cases} \quad (2)$$

The resulting matrix **D** maps all discovered holes in the ΔDEM. According to the smoothness of **M** w.r.t. ΔDEM, once adequate thresholds *w* and δz_{cav} have been established, commission errors are very unlikely. On the other hand, small losses of material could not be detected, but they are irrelevant.

4.2.2 Improvement of the holes contours. A further procedure has been applied to better define the contours of each cavity and to improve the accuracy of the computed detached volumes. Indeed, errors in the classification of contours by linear filtering might be larger when the depth of the holes is deeper. For this reason a median filtering is applied only to redefine contours of already extracted holes, not to look for new ones. Results of latest filtering are stored into a matrix **M′**. Now the test (2) is applied again but considering **M′** instead of **M**. After the second classification, the contour of each hole is redefined.

4.2.3 Output map generation. Finally the change detection stage is ended and the final map of detached boulders can be plotted in 2-D on the ΔDEM by using the map matrix **D**.
Thank to a final clustering of points belonging to the same hole, specific information (average diameter, volume, areas,...) on each of them can be exported and analyzed into a GIS/CAD environment.

4.3 Algorithm of deformation analysis

As mentioned before, the approach for deformation measurement proposed in (Lindenbergh and Pfeifer, 2005) has been extended to irregular surfaces like rock faces by analyzing the ΔDEM. Points that are close among one another are expected to follow the same stochastic behaviour and can be considered as a sample of a 1-D random variable describing the elevations of the ΔDEM. On the other hand, once vegetation has been filtered out (Sect. 3) and holes due to rock falls located.
The algorithm to detect deformations is described in the following items, with reference to workflow in figure 1.

4.3.1 Parameter selection. The analysis requires the following parameters, which play a key-role: *width of the averaging window* (w_{def}) which defines the size of each sample adopted to compute deformations; the *spacing* (Δw) between adjacent sample windows (see Fig. 7); the *minimum number of valid points* (n_w) to be averaged in each sample. In general the size of the averaging window was usually selected in the range 30-50 times the grid step δ_{DEM}, while $\Delta w = w_{def}$, and n_w=50.

4.3.2 Windowing of ΔDEM. **A** given number of averaging windows are applied to ΔDEM, according to parameters w_{def} and Δw parameters. Each window will yield a deformation measurement $\delta z_w(r,s)$ in the nearby of points (r,s) on the ΔDEM, which is the mean of the height (z) of all valid points (n_{val}). A point is valid according to its value in the mapping matrix **D**. To avoid of considering windows with too few valid points, the deformation analysis is carried on only if $n_{val} > n_w$.

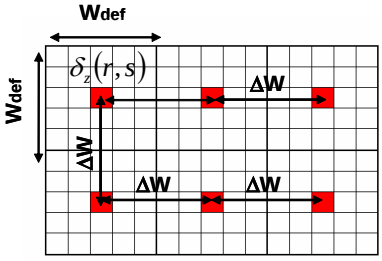

Fig. 7. Example of averaging windows to computed the mean deformation $\delta z_w(r,s)$ on a square area on the ΔDEM.

4.3.3 Standard deviation of each deformation value. The evaluation of the statistical significance of each $\delta z_w(r,s)$ also requires to know the corresponding std-dev. σ_w. Each averaging window is considered as a sample of correlated data, thus the variance of the mean value is computed under this hypothesis. Correlations arise because: (i) points of both DEMs come out from an interpolation process; (ii) points of each DEM derive from the same point cloud, then they are affected by similar georeferencing errors and might have been influenced by the same environmental conditions during acquisition.
The variance of each element is evaluated from the accuracy of each laser point measurement in both point cloud, considering that other preliminary steps (interpolation, generation of the ΔDEM worsen the accuracy) might increase the uncertainty.
An analytical analysis of correlations is really complex and has been omitted. An alternative approach has been tried by computing an empirical *autocorrelation* function (Scaioni and Alba, 2010). In practical applications, correlations are omitted but the variance of the sample mean is multiplied by a magnifying security coefficient (usually 2).
The relevance of σ_w is obvious, because the lower is its value, the higher is the possibility to detect also very small deformations.

4.3.4 Testing the computed deformation. the H_0 hypothesis is that no deformation occurred (i.e. δz_0=0); then the statistic $\xi = (\delta z_w(r,s) - \delta z_0)/\sigma_w \approx N(0,1)$ is tested. Given a risk α and the corresponding critical value $\xi_{\alpha/2}$, H_0 is rejected if $|\xi| > \xi_{\alpha/2}$.
It is then possible to fix in each window a minimum threshold for the acceptance of a significant deformation:

$$\delta z_{def} = \sigma_w \cdot \xi_{\alpha/2} \quad (3)$$

5. RESULTS

The change detection and deformation algorithms presented here were initially tested on a synthetically generated data set that was also used to set the different thresholds of the input parameters and to validated the algorithmic efficiency. All the test results have been reported in Scaioni and Alba (2010). Here we limit to present only results on application to a real dataset.

First of all, both point clouds acquired and georeferenced at two different epochs were preprocessed as explained in subsection 4.1, and afterwards each region Reg_k was analyzed. For the example only a region of 4.2x8.3 m with a strong presence of detachments was investigated. Input thresholds and internal parameters are shown in table 1.
Here the application of the Change Detection algorithm was successful to identify 5 detachments, for a total volume of 0.035 m^3. The results of the search for detachments were partially validated by recovering of some pieces of rocks corresponding to the detected holes in the ΔDEM. The deformation analysis showed displacements of a few tenths of a millimetre, that however were not considered as statistically significant (Fig. 8).

Parameters	# δ_{DEM}	cm
w_{cav}	2	10
δz_{cav}	1	5
w_{def}	4	20
Δw	4	20
σ_z	±0.01	±0.5
δ_{DEM}	1	5
$n_w(\%)$	90	

Tab. 1. Input thresholds adopted in the processing.

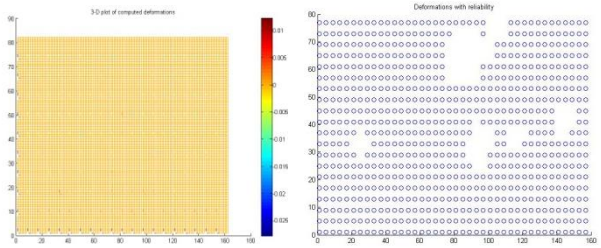

Fig. 8. Results of the deformation (left) and statistical significance (right) analysis, where blue circles indicates the centre of windows where displacements were tested as insignificant.

6. CONCLUSIONS

In the paper the whole workflow for monitoring a rockface and to detect changes and deformation of its surface has been outlined. All the processing steps have been briefly discussed, while details can be found in other related articles.
In particular, here two problems have been discussed and solutions have been proposed and tested. The problem of *vegetation filtering* has been addressed by a new method based on NIR images captured by a camera integrated to TLS. This technique seemed to be very promising, but unfortunately it could not be fully validated yet.
Secondly, a method for *change detection* and *deformation analysis* on multi-temporal digital surfaces of rock faces has been presented. The achievable results are a map of fallen blocks and a map of deformations. The process is highly automatic and will offer to experts on rockfall forecasting a powerful tool for an integrated analysis.
On the other hand, the complexity of the sites with high rock fall risk would require further experimentations and validation. Probably, some steps of the processing pipeline summarized in figure 1 should be tuned and modified to cope with specific local situations.

ACKNOWLEDGEMENTS

Authors would like to gratefully aknowledge Laura Longoni and Monica Papini (Politecnico di Milano) for suggesting the test site location. Aknowledgements also go to Riccardo Roncella (Università di Parma, Italy) for point cloud segmentation.

REFERENCES

Abellán, A., Jaboyedoff, M., Oppikofer, T. and Vilaplana, J., 2009. Detection of millimetric deformation using a terrestrial laser scanner: experiment and application to a rockfall event. Nat. Hazards Earth Syst. Sci. 9, pp. 365-372.

Abellán,, A., Vilaplana, J. and Martínez, J., 2006. Application of a longrange terrestrial laser scanner to a detailed rockfall study at Vall de Nuria(Eastern Pyrenees, Spain). Eng. Geology 2006(88), pp. 136-148.

Alba M., Roncoroni F. and Scaioni M., 2008. Investigations about the Accuracy of Target Measurement for Deformation Monitoring. In: IAPRSSIS 37(B5), Beijing, China, pp. 1053-1059.

Alba, M., Roncoroni, F. and Scaioni, M., 2009. Application of TLS for change detection in rock faces. In: IAPRSSIS 38(3/W8), Paris, France, pp. 99-104.

Arosio D., Longoni, L., Papini, M., Scaioni, M., Zanzi, L., Alba, M., 2009. Towards rockfall forecasting through observing deformations and listening to microseismic emissions. Nat. Hazards Earth Syst. Sci. 9, pp. 1119-1131.

Labbé, S., Roux, B., Bégué, A., Lebourgeois, V. and Mallavan, B., 2007. An operational solution to acquire multispectral images with standard light cameras: characterisation and acquisition guidelines. In: IAPRSSIS, Newcastle, UK, 11-14 Nov 2007.

Lindenbergh, R. and Pfeifer, N., 2005. A statistical deformation analysis of two epochs of terrestrial laser data of a lock. In: Proc. of the 7th Conf. on Optical 3-D Measurement Techniques, Vol. 1, Vienna, Austria, pp. 61-70.

Roncella, R. and Forlani, G., 2005. Extraction of planar patches from point clouds to retrieve dip and dip direction of rock discontinuities. In: IAPRSSIS 36(3/W19), Enschede, The Netherlands, pp. 162-167.

Scaioni M. and Alba, M., 2010. Understanding changes and deformations on multi-temporal rock face point clouds. In printing in: IAPRSSIS, Paris, France, 6 pp..

Schneider, D., 2006. Terrestrial laser scanning for area based deformation analysis of towers and water dams. In: Proc. of '3rd IAG Symp. on Deformation Measurements and Analysis'/'12th FIG Symp. on Geodesy for Geotechnical and Structural Eng.', Vol. 1, Baden, Austria, 10 pp..

Teza, G., Galgaro, A., Zaltron, N. and Genevois, R., 2007. Terrestrial laser scanner to detect landslide displacement field: a new approach. Int.J. Remote Sens. 28(16), pp. 3425-3446.

Tucker C. J., 1979, Red and photographic infrared linear combinations for monitoring vegetation. Remote Sensing of Environment 8, pp. 127-150.